Fate of Atmospheric Particles within the Buddhist Cave Temples at Yungang, China

Christos S. Christoforou, Lynn G. Salmon, and Glen R. Cass

Mechanical Engineering Department and Environmental Quality Laboratory, California Institute of Technology, Pasadena, California 91125

ENVIRONMENTAL® SCIENCE & TECHNOLOGY

Reprinted from
Volume 30, Number 12, Pages 3425–3434

Environ. Sci. Technol. 1996, 30, 3425–3434

Fate of Atmospheric Particles within the Buddhist Cave Temples at Yungang, China

CHRISTOS S. CHRISTOFOROU, LYNN G. SALMON, AND GLEN R. CASS*

Mechanical Engineering Department and Environmental Quality Laboratory, California Institute of Technology, Pasadena, California 91125

The Yungang Grottoes are a collection of man-made cave temples dating from the 5th century A.D. that now are situated in the middle of one of China's largest coal mining regions. Air pollutant particles enter these caves and deposit onto the more than 50 000 stone carvings contained within the caves, leading to rapid soiling of the sculptures. In order to study this problem, computer-based models have been combined that simulate the air flow into the caves and particle deposition within the caves. The evolution of the airborne particle concentration and size distribution is tracked as outdoor air is drawn into the caves by a natural convection flow that is driven by the temperature difference between the outdoor air and the interior walls of the caves. Particle deposition rates are computed from the boundary layer flows along the surfaces within the caves. Predicted coarse airborne particle (diameter > 2.3 μm) size distribution and coarse particle deposition fluxes to horizontal surfaces within caves 6 and 9 at Yungang compare closely to experimental observations made during the period April 15–16, 1991. It is found that horizontal surfaces within caves 6 and 9 at Yungang would become completely covered by a full monolayer of particles in only 0.3–0.5 yr under the April conditions studied here and will be soiled even more rapidly under annual average conditions. The model developed here can be used in the future to compute the effects of particle filtration systems and/or altered ventilation rates on soiling within the grottoes.

Introduction

Archaeological sites that are exposed to a polluted atmosphere can be damaged as a result. One such site that suffers from a very high rate of airborne particle deposition is the collection of more than 20 Buddhist cave temples at Yungang in northern China. The Yungang Grottoes are carved into the side of the Wuzhou Hills, about 16 km west of the industrial city of Datong, in the north of Shanxi Province. The earliest caves were excavated into the face of a sandstone cliff under the patronage of the emperors of the Northern Wei Dynasty (*1*) during the middle of the 5th century A.D. Cross-sectional drawings of caves 6 and 9 at Yungang, which will be discussed extensively in the present work, are shown in Figure 1, and a color photograph of the cliff face at Yungang showing caves 6 and 9 at the right taken during the experiments reported here is reproduced by Holloway (*2*). Many of the caves consist of an interior chamber of approximate plan size of 12 m by 12 m by 15 m high, hollowed out around a central column that typically is carved into a giant statue of the Buddha or alternatively takes the shape of a pagoda. More than 50 000 smaller Buddhist carvings adorn the interior walls of the caves and depict Buddhist deities or scenes from the life of the Buddha. In antiquity, the entrances to each large cave were covered by a wooden temple structure several stories high and one room deep, as seen in front of cave 6 shown in Figure 1. Significant repairs to the caves were made during the 11th and 17th centuries. By the early 20th century, travelers to the area report that the caves had fallen into a state of neglect (*3*), and by that time only caves 5 and 6 retained a wooden structure in front of their entrance. In more recent years, the caves have been cleaned, and their surroundings have been turned into a park. Hundreds of visitors daily visit the site.

Today, Yungang is surrounded by one of China's largest coal mining regions. Particles are generated by the various processes at the mines. Coal truck traffic on a nearby highway produces much dust. Coal combustion occurs for cooking and heating in the village of Yungang. Coal-fired locomotives run on nearby railroad tracks. Traffic on dirt roads in the village of Yungang creates additional dust. Since Yungang is located near the edge of the Gobi Desert, it also is affected by regional dust storms. As a result of a combination of the above, the Yungang Grottoes suffer from a severe particle deposition problem, and the statues and carvings inside the caves are soiled at a rapid rate.

From a year-long monitoring program conducted during 1991/1992 (*4*), the following background information can be provided:

(a) The outdoor airborne particle concentrations at Yungang are very high. Annual average coarse (diameter, $d_p > 2.1\,\mu$m) particle concentrations outdoors during 1991–1992 averaged 378 μg m^{-3}, increasing to more than 1200 μg m^{-3} during peak 24-h sampling periods while fine airborne particle concentrations ($d_p \leq 2.1\,\mu$m) outdoors averaged 130 μg m^{-3} (*5*).

(b) The largest contributors to the coarse airborne particles include crustal dust (e.g., soil dust), accounting for over 80% of the coarse particle mass, and carbon-containing particles (10% of coarse mass). The fine particles outdoors consist of carbon-containing particles (45.5%) followed in importance by crustal dust (24%) (*5*).

(c) The outdoor particles are transferred to the inside of the caves by a natural convection flow (*6*). As seen in Figure 1, the largest caves at Yungang contain two entrances through the stone cliff face, one at ground level (position 1 in Figure 1a and position 2 in Figure 1b) and a second entrance at about the third floor level (position 2 in Figure 1a and position 3 in Figure 1b). During the middle of the day, the outdoor air is warmer than the cave walls. As a

* To whom all correspondence should be addressed.

S0013-936X(95)00875-3 CCC: $12.00

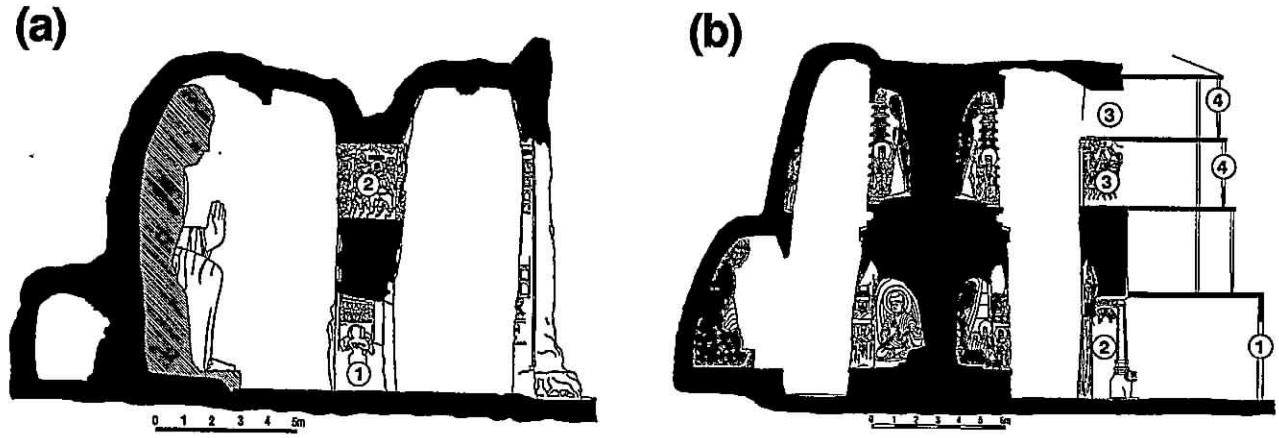

FIGURE 1. Vertical cross section drawings of cave 9 (a) and cave 6 (b).

result, air enters the caves through the upper windows in the cliff face, cools as it flows down the colder interior cave walls, and then exits through the ground level entrance to the cave. At night, the reverse happens: cold outdoor air flows into the caves through the ground floor entrance, flows up the warmer walls, and flows out of the caves through the opening in the rock face of the cliff at about the third floor level.

(d) Once inside the caves, the airborne particles deposit onto the various horizontal and vertical surfaces. For example, measurements show that over the 5-yr period from 1986 to 1991, particle deposits as deep as 0.8 cm, with an average depth of 0.4 cm, accumulated on the sculptures within cave 9 at Yungang (*4*).

In order to test the design of systems that will control this particle deposition problem, a quantitative description of the cause and effect relationships that translate outdoor particle concentrations into the observed deposition flux is needed. In this paper, a computer-based mathematical model will be formulated that links the outdoor particle concentration and size distribution and the air flow through the caves to the indoor particle concentration and size distribution. The particle flux to interior surfaces will be simulated along with the determination of the rate of surface coverage by depositing particles. The model will be tested using detailed measurements of the time series of outdoor particle size distributions and indoor particle concentrations and deposition fluxes within caves 6 and 9 at Yungang during April 1991. Once verified, this model can be used to study the effect of proposed particle filtration and control systems for the caves in advance of their adoption.

Model Formulation

The airborne particle deposition model for the Yungang Grottoes is constructed by combining the features of an existing model for indoor aerosol mechanics and particle deposition in buildings with a fluid mechanical model for the natural convection-driven air exchange between the outdoors and the cave interior.

The model for the air exchange between the interior of the caves and the outdoors is based on the description of Christoforou et al. (*6*). A natural convection flow is driven by wall and air temperature differences. When warm air flows into a cave like cave 9 at Yungang, it enters through the upper level window in the rock wall at position 2 in Figure 1a. The air is cooled as it flows down the cave walls; cool air accumulates in the cave and then flows out of the ground level entrance to the cave at position 1 in Figure 1a. Three equations can be written that describe the simultaneous convection and heat transfer problem at cave 9:

$$\frac{d}{dt}(\rho_a V) = \rho_o U_2 A_2 - \rho_a U_1 A_1 \quad (1)$$

$$\frac{d}{dt}(\rho_a V c_v T_a) = \rho_o U_2 A_2 c_p T_o - \rho_a U_1 A_1 c_p T_a - \sum_{i=1}^{3} h_i S_i (T_a - T_w) \quad (2)$$

$$\frac{1}{2}\rho_o U_2^2 C_L + \frac{1}{2}\rho_a U_1^2 C_L = gH(\rho_a - \rho_o) \quad (3)$$

where ρ_a is the mass density of air inside the cave; ρ_o is the mass density of air outside the cave; V is the volume of the cave; U_1 and U_2 are the air velocities through the openings in the rock wall between the outdoors and the inside of the cave at positions 1 and 2 in Figure 1a, respectively; T_a and T_o are the temperatures of the air inside the cave and the air outdoors, respectively; T_w is the temperature of the cave walls; c_p is the specific heat of air measured at constant pressure; c_v is the specific heat of air measured at constant volume; A_1 and A_2 are the cross-sectional areas of the openings through the rock wall at positions 1 and 2 in Figure 1a; h_i is the heat transfer coefficient for flow over the ith surface inside the cave where index i runs from 1 to 3 indicating walls, floor, and ceiling, respectively; S_i is the surface area of the ith surface inside the cave; C_L is the loss coefficient for flow through the rectangular openings in the rock wall at positions 1 and 2 in Figure 1a; H is the elevation difference between the entering and exiting portions of the critical fluid streamline along which motion starts as air enters and leaves the cave, and g is the acceleration due to gravity. Equations 1–3 describe continuity, energy conservation, and the balance between the pressure drops in the air path versus density differences acting on the height of the air column between the entering and exiting air paths, respectively.

This system of equations is then simplified by assuming that $\rho_a \approx \rho_o \approx \rho$ except that $(\rho_a - \rho_o)/\rho_o \neq 0$, and also $(\rho_a - \rho_o)/\rho_o \approx (T_o - T_a)/T_o$, so that eqs 1–3 become

$$U_1 A_1 = U_2 A_2 \quad (4)$$

TABLE 1

Natural Convection Heat Transfer Relationships used by Transport Algorithm of Particle Deposition Model

surface	Nusselt number[a]	condition	ref
vertical walls	$\overline{Nu}_Z = \left(0.825 + \frac{0.387 Ra_Z^{1/6}}{[1 + (0.492/Pr)^{9/16}]^{8/27}}\right)^2$	$10^{-1} < Ra_Z < 10^{12}$	*b*
horizontal			
upward facing heated or downward facing cooled surface	$\overline{Nu}_L = 0.54 Ra_L^{1/4}$	$10^4 < Ra_L < 10^7$	*c*
	$\overline{Nu}_L = 0.15 Ra_L^{1/3}$	$10^7 < Ra_L < 10^{11}$	*c*
horizontal			
upward facing cooled or downward facing heated surface	$\overline{Nu}_L = 0.27 Ra_L^{0.25}$	$10^5 < Ra_L < 1.4 \times 10^{10}$	*c*

[a] $\overline{Nu}_Z = Zh_i/k$ is the Nusselt number based on the height of the cave walls, Z; the heat transfer coefficient, h_i, along the ith surface; and the thermal conductivity of air, k. $\overline{Nu}_L = Lh_i/k$ is the Nusselt number based on a characteristic dimension, L, which is computed as the area of the surface divided by the perimeter of the surface. Ra_Z is the Rayleigh number based on the height of the cave walls. $Ra_Z = Pr\, g|T_w - T_a|Z^3/(T_a\nu^2)$, where Pr is the Prandtl number for air, g is the acceleration due to gravity, ν is the kinematic viscosity of air, T_w is the cave surface temperature, and T_a is the air temperature in the cave. Ra_L is the Rayleigh number based on the characteristic length, L, which is computed as the area of the surface divided by its perimeter. [b] From Churchill and Chu (*7*). [c] From Incropera and DeWitt (*8*).

$$\rho V c_v \frac{d}{dt}(T_a) = \rho c_p (U_2 A_2 T_o - U_1 A_1 T_a) - \sum_{i=1}^{3} h_i S_i (T_a - T_w) \quad (5)$$

$$U_1^2 + U_2^2 = \frac{2gH}{C_L} \frac{|T_o - T_a|}{T_o} \quad (6)$$

An analogous set of equations can be written for the case where cold air enters at ground level and flows up the warmer walls of the cave. Equations 4–6 may be solved for the unknown air velocities through the openings into cave 9 (U_1 and U_2) as well as the indoor air temperature (T_a) within the cave, which are the unknown parameters in this problem. Once either U_1 or U_2 is known as a function of time, the air flow through the cave is known.

In the case of a cave like cave 6, which still retains the wooden structure in front of the cave entrance, the additional pressure drops that occur as air flows through the doors and cracks in the wooden building must be simulated. The incorporation of such added pressure drops into the system of eqs 4–6 is described more fully elsewhere (*6*).

Solution of eqs 4–6 requires that the heat transfer coefficients for air flow over the various interior surfaces of the cave, the h_i in eq 5, must be estimated. Natural convection heat transfer coefficients used to represent flow over the vertical walls of the caves, the cave ceiling, and the cave floor are given in Table 1. These heat transfer coefficients were derived for flow over flat plates, but the walls of the cave are not flat. Instead they are carved in high relief. As a result, the walls contain more surface area than the superficial dimensions of the walls would indicate. The walls also contain roughness elements that will interrupt the natural convection boundary layer flow, thereby increasing heat transfer rates. To compensate for the added surface roughness and surface area, a semi-empirical adjustment to the model was developed and tested (*6*): the product $h_1 S_1$ appearing in eq 5, which quantifies heat transfer rates for flow over the vertical walls of the cave, was taken to be twice as large as would be the case for a vertical flat plate having the nominal surface area of the major outline of the cave walls. This correction was based on an examination of photographs that show that the actual surface area of the carved walls consists of hundreds of closely spaced Buddhist deities carved in high relief. We estimate that a sequence of human figures backed against a wall with spacing between the figures like that seen at Yungang yields about a factor of 2 greater surface area than the superficial area computed from the wall perimeter times the cave height.

Particle Deposition Model. The model for particle deposition onto surfaces within the caves follows the formulation of Nazaroff and Cass (*9*). The interior of each cave is represented as a single chamber having a well-mixed core. The aerosol within the cave is represented by the multicomponent sectional formulation of Gelbard and Seinfeld (*10*). The particle size distribution is divided into 22 consecutive bins that cover the range from 0.05 to 149.7 μm in diameter. Particles of each size may be composed of many different chemical components, but all particles of the same size have the same relative composition (i.e., the aerosol is assumed to be internally mixed). The aerosol mass concentration within each size section is assumed to be uniformly distributed with respect to the logarithm of the diameter of the particles. The rate of change of the aerosol mass concentration for each component within each size section is governed by the following differential equation:

$$\frac{d}{dt} C_{mjk} = S_{mjk} - L_{mjk} C_{mjk} \quad (7)$$

where C_{mjk} represents the mass concentration of chemical component k in particle size section j within chamber m of the model; S_{mjk} is the sum of all sources of component k in particle size j within chamber m, and L_{mjk} is the sum of all losses of component k in particle size j within chamber m. Sources (S_{mjk}) include all processes that add to the particle concentration in a size section: direct emissions of particles within the cave, advection of particles into the cave from outdoors, and coagulation of smaller particles to form larger particles. Particle losses (L_{mjk}) include deposition of particles onto surfaces, removal of particles from the caves by the natural convection flow that exits the cave, and loss of particles to larger sizes by coagulation. These sources and sinks vary over time.

While the model has the ability to handle coagulation calculations, that feature is not used during the present simulations because the fine particle concentrations are not high enough to cause that process to have important effects on the calculated aerosol size distribution. There-

TABLE 2

Particle Deposition Velocities (v_d) If Induced by Homogeneous Turbulence in Air in Core of Cave (*9*)

surface orientation	deposition velocity[a]	conditions
all	$v_d = v_{CP} + v_t$	all
all	$v_t = -N_t \nu \frac{(K_e/\alpha)^{1/2}}{\tan^{-1}(\delta(K_e/\alpha)^{1/2})}$	all[b]
vertical	$v_{CP} = \frac{2}{\pi}(DK_e)^{1/2}$	*c*
downward facing	$v_{CP} = \frac{v_g}{\exp\left(\frac{\pi v_g}{2(DK_e)^{1/2}}\right) - 1}$	*c*
upward facing	$v_{CP} = \frac{v_g}{1 - \exp\left(\frac{-\pi v_g}{2(DK_e)^{1/2}}\right)}$	*c*

[a] In the equations above, v_{CP} is the deposition velocity according to Corner and Pendlebury (*11*); v_t is the thermophoretic velocity of particles; $N_t = K(\Delta T/T_\infty)$ is the thermophoresis parameter; ΔT is the temperature difference between the surface temperature and the temperature of air outside the boundary layer, T_∞; K_e is the turbulence intensity parameter; K is the thermophoresis coefficient (*12*); D is the coefficient of Brownian diffusivity of particles; α is the thermal diffusivity of air; and v_g is the gravitational settling velocity. [b] In the expression for deposition velocity, δ is the boundary layer thickness given approximately by $\delta \sim (1.2)(\nu/K_e)^{4/9}x_s^{1/9}$, where x_s is the length of the surface in the direction of flow (*9, 12*), and ν is the kinematic viscosity of air. [c] For very small particles, v_{CP} to a surface having any orientation is more accurately given by the expression $v_{CP} = (DK_e)^{1/2}/[\tan^{-1}[\delta(K_e/D)^{1/2}]]$, where δ is given in footnote a above. For a particle to be sufficiently small for this expression to be appropriate, it must satisfy $D \geq 0.01\nu^{8/9}K_e^{1/9}x_s^{2/9}$. A typical set of conditions has $K_e = 0.1\ s^{-1}$ and $x_s = 1$ m, for which the inequality becomes $D \geq 0.004\ cm^2\ s^{-1}$, i.e., that the particle must be smaller than 0.004 μm in diameter.

fore, when a cave is represented by a single chamber model as it is affected by advection of air through the caves, indoor sources, and particle deposition, eq 7 becomes

$$V\frac{d}{dt}(C_{ajk}) = C_{ojk}f_{oa} + E_{ajk} - C_{ajk}\sum_i S_i v_{d_{ijk}} - C_{ajk}f_{oa} \qquad (8)$$

where C_{ajk} and C_{ojk} are the concentrations of chemical component k in particles of size j in air inside (a) or outside (o) the cave, respectively; f_{oa} is the volumetric flux of air flowing from outside to inside the cave (flow in = flow out in this case); E_{ajk} is the emission of new particles of composition k and size j due to activities within the cave, S_i is the surface area of the ith surface; and $v_{d_{ijk}}$ is the deposition velocity for particles containing component k in size j to the ith surface within the cave. In the present model application, particle emissions within the cave will be taken to be zero since the caves were unoccupied during the experiments related here. In the future, if visitors to the caves introduce a new source of particles within the caves, then the model can be readily adapted to study that situation.

Particle deposition from the atmosphere inside the caves to horizontal and vertical surfaces in the caves is calculated for the relevant air flow regimes along the interior surfaces, including deposition of particles due to turbulence in the core of the caves plus natural convection flows along the walls, as well as deposition to horizontal surfaces by both gravitational sedimentation and convective diffusion. The relationships used for computing these deposition velocities are given in Tables 2 and 3. The deposition velocity due to gravitational sedimentation used in the present work is corrected using an appropriate shape factor to account for the irregular shape of the coarse mineral dust particles encountered (*13*).

The mean particle deposition velocity to vertical surfaces depends on particle transport in the atmospheric boundary layer near the wall. Two cases are distinguished, namely, laminar or turbulent natural convection induced by the wall-air temperature difference and homogeneous turbulence induced by air movement in the core of the cave. The equations used for the former case arise from analogies between heat and mass transfer results and are fully described by Nazaroff and Cass (*9, 12, 14*). The equations used in the latter case are based on the work by Corner and Pendlebury (*11*). Both cases are discussed more fully elsewhere (*9, 14*). As was the case with the natural convection heat transfer calculations to the vertical walls of the caves described earlier, a semi-empirical correction that accounts for the added surface area of the vertical cave walls due to the carvings that are present was applied to the particle deposition calculations. The product of the deposition velocity times the surface area of the vertical walls was taken to be twice that estimated for deposition to a flat surface having an area equal to that computed from the major outline of the cave walls. This increase in effective surface area is based on detailed examination of photographs of the cave walls showing the degree of surface modulation provided by the carvings.

Inputs required for use of the model defined by eqs 4–6 and 8 are as follows: (1) the particle size distribution and concentration in the outdoor air as well as the initial particle size distribution and concentration inside the caves; (2) wall and air temperature data from which are calculated (a) the air flow into the caves by natural convection and (b) the deposition velocities of particles from natural convection flows along the walls; (3) an estimate of the turbulence intensity levels inside the caves as well as the thermophoresis coefficient for the particles (*9, 14*); and (4) the geometry and size of the caves. Measured air flows into and out of the caves can be substituted for the flows predicted by eqs 4–6 if desired. Outputs from the model include (1) the aerosol size distribution and concentration inside the caves and (2) particle deposition rates as a function of particle size to walls, floors, ceilings, and other horizontal or vertical surfaces inside the caves, from which mass fluxes and the rate of surface coverage by deposited particles can be calculated.

Experimental Program

During April 1991, an experimental program was conducted at Yungang to gather data needed for evaluation of the present model for particle deposition in the caves. The experiment extended over 2 days with samples taken over consecutive 4-h intensive sampling periods. The experiment began at 0200 h on April 15 and lasted until 2200 h on April 16. During this period, the following measurements were made:

Outdoor and Indoor Airborne Particle Concentrations and Size Distributions. Ambient aerosol samples were taken over consecutive 4-h sampling periods both outdoors and inside caves 9 and 6 by drawing air at a rate of 3 L min^{-1} through 47 mm diameter Millipore filters (0.22 μm pore size, membrane filter GSWP04700) secured in open-faced filter holders, thus ensuring collection of both large and small particles. Subsequent automated optical microscopy analysis (*4*) yielded size distributions of the

TABLE 3

Particle Deposition Velocities (v_d) for Deposition from Natural Convection Flows (*9*)[a]

surface orientation	deposition velocity	conditions
vertical	$v_d = {}^4/_3(g\lvert\Delta T\rvert/4\nu^2 T_\infty)^{1/4}\alpha^{1/3}D^{2/3}Z^{-1/4}[\omega'(0)/Le^{1/3}]$	$Ra_Z < 10^9$
	v_d = maximum of $^4/_3(g\lvert\Delta T\rvert/4\nu^2 T_\infty)^{1/4}\alpha^{1/3}D^{2/3}Z^{-1/4}[\omega'(0)/Le^{1/3}]$	$10^9 < Ra_Z < 10^{12}$
	or $v_t + \frac{D}{Z}\left\{0.825 + \frac{0.387\,Ra_Z^{1/6}}{[1+(0.492/Sc)^{9/16}]^{8/27}}\right\}^2$;	
	where $v_t = -N_t\frac{\nu}{Z}\left\{0.825 + \frac{0.387\,Ra_Z^{1/6}}{[1+(0.492/Pr)^{9/16}]^{8/27}}\right\}^2$;	
horizontal upward-facing heated or downward-facing cooled surface	$v_d = s_g v_g - N_t\nu/L(0.54Ra_L^{1/4}) + D/L(0.54Ra_L^{1/4})$	$v_d \geq 0$; $10^4 < Ra_L < 10^7$
	$v_d = s_g v_g - N_t\nu/L(0.15Ra_L^{1/3}) + D/L(0.15Ra_L^{1/3})$	$v_d \geq 0$; $10^7 < Ra_L < 10^{11}$
horizontal upward-facing cooled or downward-facing heated surface	$v_d = s_g v_g - N_t\nu/L(0.27Ra_L^{1/4}) + D/L(0.27Ra_L^{1/4})$	$v_d \geq 0$; $10^5 < Ra_L < 10^{10}$

[a] v_d is the deposition velocity; g is the acceleration due to gravity; ΔT is the temperature difference between the cave surface temperature and the temperature of air outside the boundary layer, T_∞; ν is the kinematic viscosity of air, α is the thermal diffusivity of air; D is the coefficient of Brownian diffusivity of particles; Z is the height of the cave; $\omega'(0)$ is the slope of the normalized particle concentration at the surface (*12*); Le is the particle Lewis number, α/D; v_t is the thermophoretic velocity of particles; Ra is the Rayleigh number; Sc is the particle Schmidt number, ν/D; $N_t = K(\Delta T/T_\infty)$ is the thermophoresis parameter; K is the thermophoresis coefficient (*12*); v_g is the gravitational settling velocity; s_g is an orientation coefficient, 1 for upward-facing and −1 for downward-facing; and L is a characteristic dimension of the surface (area divided by perimeter).

particles suspended in the air. This method was used to measure the size distribution of coarse airborne particles both inside and outside the caves over the diameter, d_p, range 2 μm < d_p < 148 μm. The outdoor size distribution of fine particles over the size range 0.05 μm < d_p < 2.3 μm was obtained using a 32-channel Particle Measuring Systems Model ASASP laser optical particle counter (OPC). Gravimetric determination of aerosol mass concentration, both outdoors and within the caves over each 4-h sampling period, was obtained with the use of samples collected on Teflon membrane filters (Gelman Teflo, 0.5 μm pore size) through which air was drawn at a rate of 10 L min^{-1} each. Fine particle samples were collected on a Teflon filter located downstream of an AIHL-design cyclone separator that removed particles with an aerodynamic diameter greater than 2.1 μm (*5*), while total aerosol samples were collected simultaneously on an open-faced Teflon filter. The Teflon filters were weighed before and after sampling for gravimetric determination of aerosol mass concentration. Coarse particle concentrations were determined by the difference between total particle minus fine particle concentrations.

Indoor Particle Deposition Flux onto both Vertical and Horizontal Surfaces. Millipore filters (47 mm in diameter, 0.22 μm pore size, membrane filter GSWP04700) were used as a surrogate surface for the collection of particles that deposited onto horizontal surfaces, while particles that deposited onto vertical surfaces were collected on microscope glass slides (75 mm by 25 mm by 1 mm thick). The vertical collection plates within caves 9 and 6 were fastened to the surface of a large aluminum plate, which was then secured on the cave wall in order to achieve thermal contact with the wall surface. The horizontal deposition plates were placed on top of platforms at a height of about 1 m above ground level. A pair of horizontal collection plates was exposed for each of the consecutive 4-h sampling periods on April 15–16, while a single set of vertical deposition plates was continuously exposed for the 19-day period from April 12 until April 30 because of the great difference in deposition rates between horizontal and vertical surfaces (*15*). The deposited coarse particle size distribution on both horizontal and vertical surfaces was obtained by automated optical microscopy analysis, and the results are reported by Christoforou et al. (*4*).

Temperature Data. Wall and air temperatures were measured by thermistor arrays that were placed inside caves 6 and 9 at Yungang. The wall thermistors (Part No. 44202, Yellow Springs Instrument Co., Yellow Springs, OH) were secured in wall cracks using a thermal joint compound in order to ensure proper thermal contact with the wall. The air temperature thermistors were placed 5.1 cm away from the wall. Signal conditioning circuits transformed the thermistors' output into a voltage that was proportional to the temperature. Data were recorded every minute with the aid of a Campbell Scientific CR-10 measurement and control module (Campbell Scientific Inc., Logan, UT), with the exception of cave 6 data, which were recorded using a strip chart recorder. The outdoor air temperature was measured at a weather station operated by the Chinese Government at Yungang that is located about 140 m south of the entrances to the caves, and the data were logged on a paper chart recorder.

Air Exchange Rates. In the case of cave 9, air exchange rates were measured with the aid of an omnidirectional velocity probe (TSI Model 1620) placed in the center of the ground level entrance of the cave. Data were again recorded every minute using the CR-10 data logger. A hand-held mechanical air velocity meter (vaneometer, Part No. 6610A4306, Whatman Labs, Hillsboro, OR) was also used at regular intervals to measure air speed and direction in the ground level entrance to cave 9. That information on the direction of air flow was used to assign the direction of flow to data taken continuously via the TSI omnidirectional velocity probe.

Air exchange rates through the entrance to cave 6 were measured using the mechanical air velocity meter and also using perfluorocarbon tracers (*16*). Tracer sources that emitted perfluorocarbons at a slow but constant rate were placed at selected locations inside the cave. Tracer collection tubes were exposed over consecutive 4-h periods and then were analyzed to give the total air infiltration rate through the cave (m^3 h^{-1}) as a function of time. Analysis

TABLE 4

Characteristics of Caves 6 and 9

symbol	description	cave 6	cave 9
S_1	wall area, m^2	1370	174
S_2	ceiling area, m^2	163	44
S_3	floor area, m^2	179	44
V	volume, m^3	2222	528
Z	physical height of the cave	15 m	10.35 m
H	elevation difference between entering and exiting critical fluid streamline	9.25 m	2.39 m
A_1	cross-sectional area of entrance through rock wall at ground level, cave 9		7.4 m^2
A_2	cross-sectional area of opening in rock wall at 3rd and 4th floor level, cave 9		5.6 m^2
A_{1a}	cross-sectional area of openings in building shell downstairs, cave 6, front door open	4.8 m^2	
A_{1b}	cross-sectional area of openings in building shell downstairs, cave 6, front door closed	0.46 m^2	
A_2	cross-sectional area of entrance through rock walls at ground level, cave 6	11.82 m^2	
A_3	cross-sectional area of opening in rock wall at 3rd plus 4th, floor level, cave 6	21.12 m^2	
A_4	cross-sectional area of openings in building shell upstairs, cave 6	4.09 m^2	
monitoring period			
start time, date		0200 h, April 15, 1991	0200 h, April 15, 1991
end time, date		2200 h, April 16, 1991	2200 h, April 16, 1991

of the tracer samples taken was performed by the Brookhaven National Laboratory staff.

Model Evaluation

The field experimental data for the April 15–16 period at Yungang were matched to the particle deposition model. Air flows and particle deposition fluxes within both cave 6 and cave 9 were computed starting from the cave dimensions given in Table 4 and the time series of measured outdoor particle size distributions plus data on the time series of the outdoor air temperatures (T_o) in eqs 5 and 6, and the indoor cave wall temperatures (T_w) in eq 5. Air flow through cave 6, which retains a wooden temple structure in front of its entrances, is modeled with the main ground level doors to that wooden structure open during the day but closed at night, as described in detail by Christoforou et al. (*6*). The outdoor airborne coarse particle concentration ($d_p > 2\,\mu m$) and outdoor airborne fine particle concentration ($d_p < 2\,\mu m$) data supplied to the model are illustrated in Figure 2. The fine particle data of Figure 2b show a comparison of consecutive 4-h average outdoor particle mass concentrations measured gravimetrically from samples collected on Teflon filters as described earlier versus the consecutive 4-h average fine particle mass concentration computed by integrating the aerosol size distribution measured by the PMS laser optical particle counter over the size range below 2.3 μm particle diameter using an assumed fine particle density of 2.2 g cm^{-3}.

The graph of outdoor coarse particle concentrations over time (Figure 2a) shows data obtained by the difference between gravimetric analysis of consecutive 4-h average total particle samples collected on open-faced Teflon membrane filters minus concurrent measurements of fine particle concentrations compared to coarse particle mass concentrations estimated by automated light microscopy analysis of particles larger than 2 μm diameter collected on Millipore filters. Conversion of particle counts to mass concentrations for those coarse particle samples was accomplished using a coarse particle density of 2.2 g cm^{-3} and a shape factor of 1.46 (*13*, *17*). The single-particle density values are based on examination of bulk deposits of formerly airborne material removed from surfaces in the caves at Yungang, and the shape factor is determined by examination of both airborne and deposited particle samples from Yungang. The aggregated deposits composed of many particles as they reside on the cave surfaces are fluffy and have a lower mass per unit volume of bulk deposit than 2.2 g cm^{-3} due to much included air space between particles. Fine particle mass concentrations measured gravimetrically are in excellent agreement with mass concentrations inferred from integration of aerosol size distribution data. Coarse particle mass concentrations measured by integrating particle size distribution data are generally lower than concentrations measured gravimetrically, but the data obtained by particle counting are still usually within ± 2 standard errors of the gravimetrically determined values.

An example of the combined outdoor airborne fine particle plus coarse particle size distribution is shown in Figure 3, averaged over the entire 2-day experiment. That size distribution is obtained by merging the fine particle data from the laser optical particle counter with concurrent coarse particle counts taken by automated light microscopy applied to the outdoor Millipore filter samples. Similar size distribution data are available for each 4-h period during the experiment, and those consecutive 4-h average size distribution data form the actual inputs to the particle deposition model.

The outdoor coarse particle concentrations shown in Figure 2 are seen to be both much higher than the fine particle concentrations and show greater variation throughout the day. These coarse particle concentrations peak at greater than 1000 $\mu g\ m^{-3}$ over the 4-h averaging period nominally extending from about 0600 h to 1000 h each morning. During the early part of this time period, activities within the small village of Yungang and along the nearby highway have begun, and broom sweeping of the dirt terrace in front of the caves is observed, but the air is generally still,

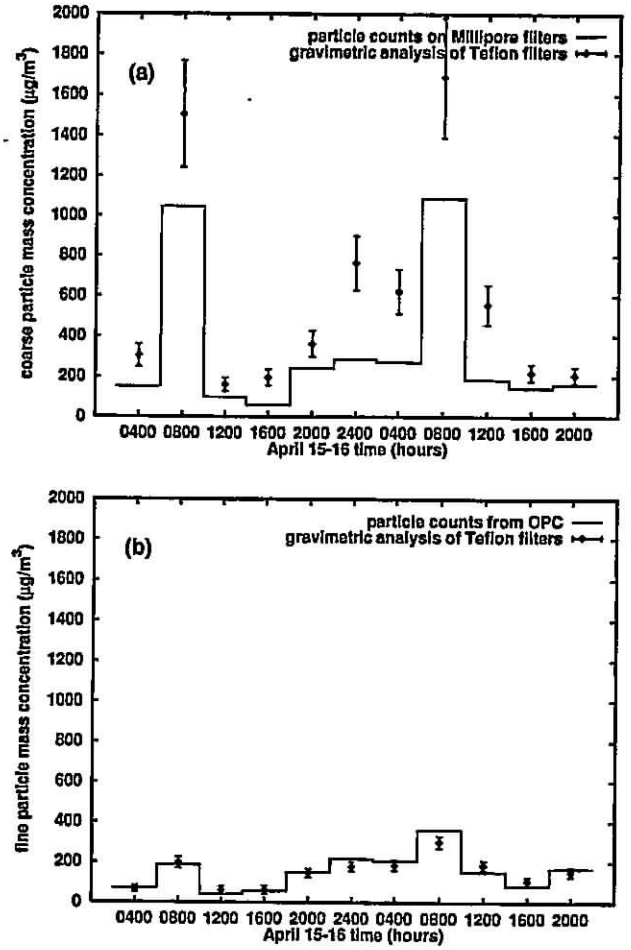

FIGURE 2. Outdoor airborne particle mass concentrations, April 15–16: (a) Coarse particle mass concentration measured gravimetrically using Teflon filters compared to mass calculated from particle counts on Millipore filters. (b) Fine particle mass concentration measured gravimetrically using Teflon filters compared to mass concentration calculated from laser optical particle counter data. Error bounds shown represent ±1 SD of the gravimetric determinations.

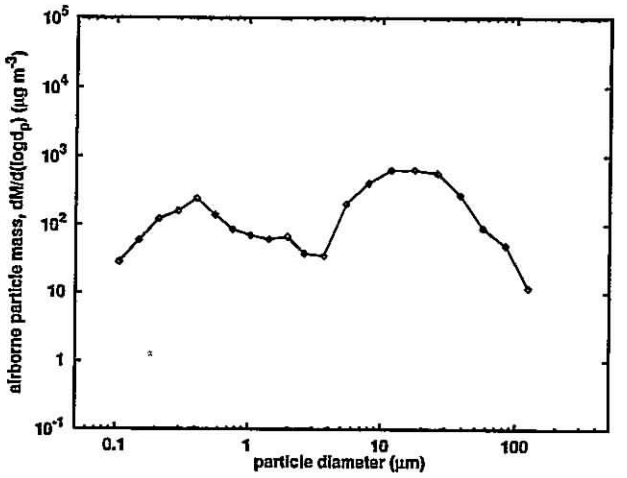

FIGURE 3. Average outdoor airborne particle mass distribution at Yungang, $dM/d(\log d_p)$, averaged over the period April 15–16, 1991. Data used for the particle size range less than 2.3 μm are from a laser optical particle counter. Concurrent data from automated optical microscopy analysis of samples collected on Millipore filters are used to determine the coarse particle size distribution ($d_p > 2.3$ μm).

and mixing depths are low, leading to high outdoor particle concentrations.

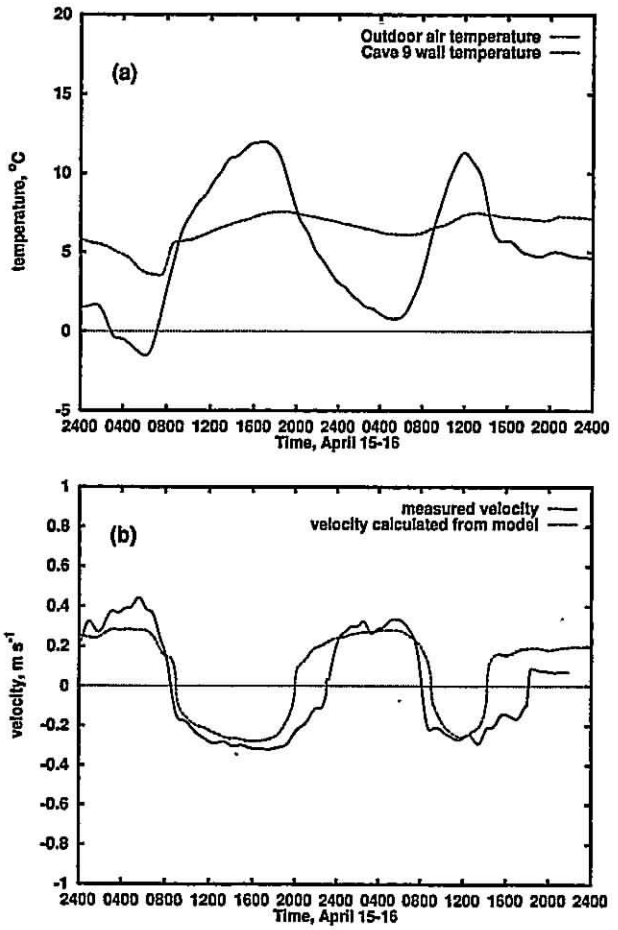

FIGURE 4. (a) Outdoor air temperature and wall surface temperature inside cave 9, April 15–16, and (b) measured air velocity at the center of the ground level entrance to cave 9, April 15–16, compared to velocity calculated from the model of eqs 4–6. A positive velocity value indicates flow into the ground level entrance to cave 9, while a negative velocity value indicates flow out of the ground level entrance at position 1 in Figure 1b.

In addition to the time series of outdoor aerosol size distribution data, the deposition model requires time series data on the outdoor air temperature and cave wall temperatures. From these temperature data, air flows through the caves are predicted. Figure 4a shows the outdoor air temperature and the cave wall temperature at cave 9 over the 2-day period studied here. Also shown is the air velocity measured after having filtered the output of the thermoelectronic velocity probe located in the ground level entrance to cave 9 at position 1 in Figure 1a as compared to the velocity predicted by the natural convection air exchange model of eqs 4–6 (see Figure 4b). A very detailed analysis of the performance of the air exchange model over a much longer period of time is provided by Christoforou et al. (6). From Figure 4, it is seen that at night when the outdoor air is colder than the cave walls, air flows into the cave at the ground level entrance (graphed as the positive flow direction in Figure 4b), while during the day the situation reverses. On most days during April 1991, air flows stagnated and then reversed direction twice per day, once at about 0930 h in the morning and again at about 2100 h at night, as is typified by the data for April 15, with both flow reversals occurring near the time of zero temperature difference between the outdoor air and the cave walls. From Figure 4b, it is seen that the natural convection air flow model for cave 9 predicts both the

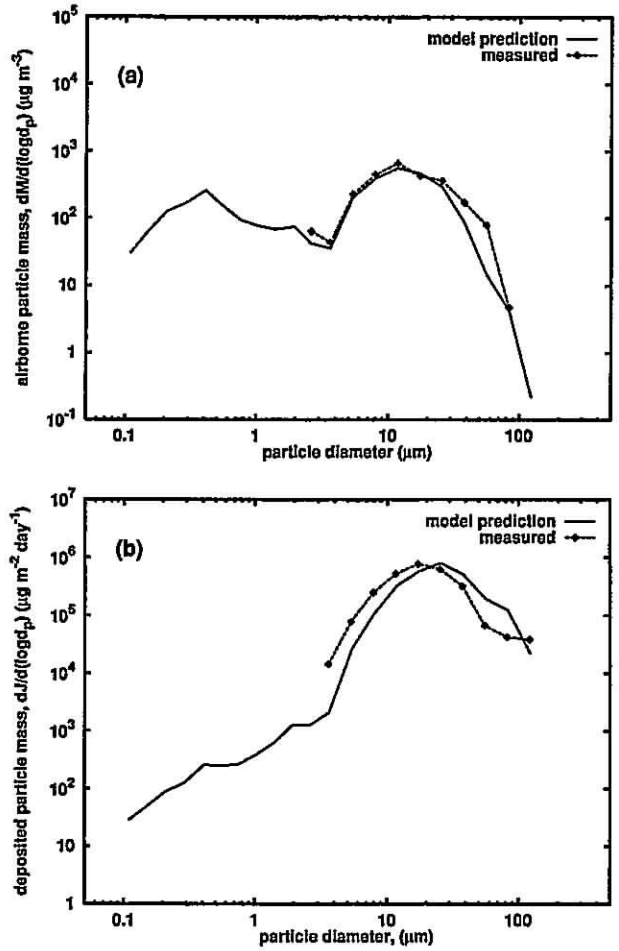

FIGURE 5. Model performance, April 15–16, cave 9: (a) Predicted 2-day average mass distribution of airborne particles, d*M*/d(log d_p), inside cave 9 compared to measured values, and (b) predicted size distribution of the particle deposition rate, d*J*/d(log d_p), onto horizontal surfaces inside cave 9 compared to measured values.

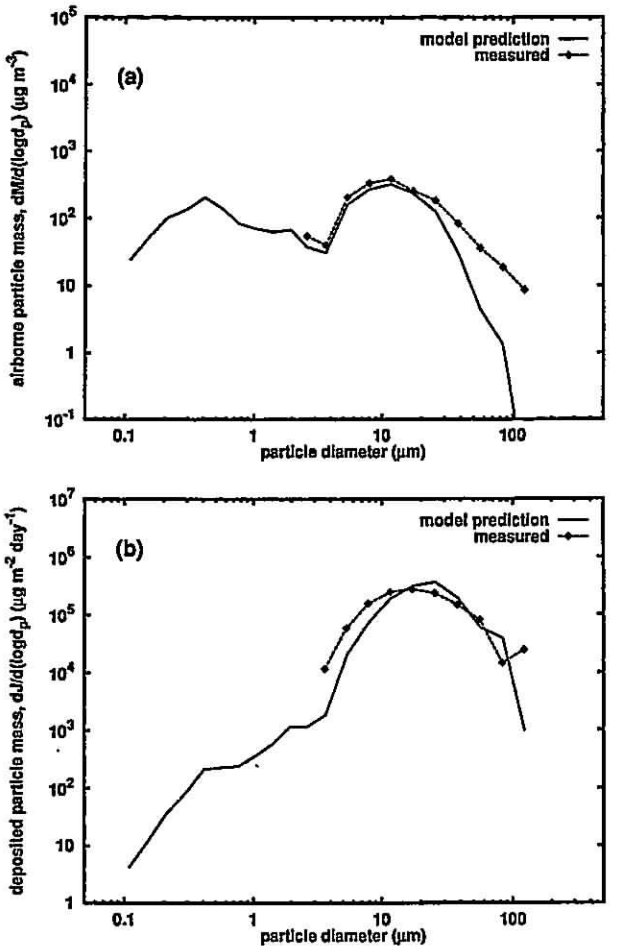

FIGURE 6. Model performance, April 15–16, cave 6: (a) 2-day average size distribution of airborne particles, d*M*/d(log d_p), inside cave 6 compared to measured values, and (b) predicted size distribution of the particle deposition rate, d*J*/d(log d_p), onto horizontal surfaces inside cave 6 compared to measured values.

pattern and the magnitude of the air flows through that cave reasonably well. Air exchange between the outdoors and the interior of cave 6 likewise is reproduced well by the natural convection model, and these results are displayed and discussed by Christoforou et al. (*6*).

Figure 5 shows model predictions of the airborne particle mass size distribution inside cave 9 averaged over the 44-h experiment as well as the size distribution of the daily average (24-h average) mass flux of particles deposited onto horizontal surfaces within cave 9 over that period. Model predictions in size ranges above 2 μm particle diameter are compared to particle counts obtained by automated optical microscopy analysis of airborne particle filter samples and deposited particle samples, both collected on the surfaces of Millipore filter material. Within cave 9, excellent agreement is obtained between measured and predicted airborne coarse particle size distributions and between the measured vs predicted size distribution of coarse particle fluxes to horizontal surfaces. Fine particle concentrations measured by filtration inside cave 9 can be compared to the integral under the predicted size distribution curve of Figure 5a in particle sizes below 2.1 μm in diameter. Averaged over the course of the 2-day simulation, the predicted airborne fine particle concentration inside cave 9 is 149 μg m^{-3} as compared to an average measured concentration of 151 μg m^{-3}.

As can be seen if Figure 6 is compared in detail to Figure 5, indoor coarse particle concentrations and deposition fluxes inside cave 6, both measured and predicted, are lower than in cave 9. This occurs in part because the average retention time for air parcels inside cave 6 is about four times longer than in cave 9. Differences in air parcel retention time between caves 6 and 9 vary by time of day. The wooden doors at the ground level entrance to the temple structure in front of cave 6 are closed both at night and during the early portion of the high outdoor coarse particle concentration episodes depicted in the morning hours in Figure 2a. When those doors are closed, air is forced to flow through the many cracks and small openings in the wooden building shell, and the added resistance to air flow causes the indoor/outdoor air exchange rate to drop. This reduced air exchange rate in turn acts to reduce particle induction into the building in front of cave 6 at those times, slowing the replacement of deposited particles, thus lowering both indoor airborne particle concentrations and particle deposition fluxes.

Figure 6 indicates that model predictions do not match measured values in cave 6 as closely as was the case inside cave 9. This is due mainly to the fact that the outdoor particle samples used to drive predictions for both cave 6 and cave 9 were collected directly in front of cave 9 (see sampler placement diagram in ref 5). Coarse particle concentrations, due to their generation by fugitive dust

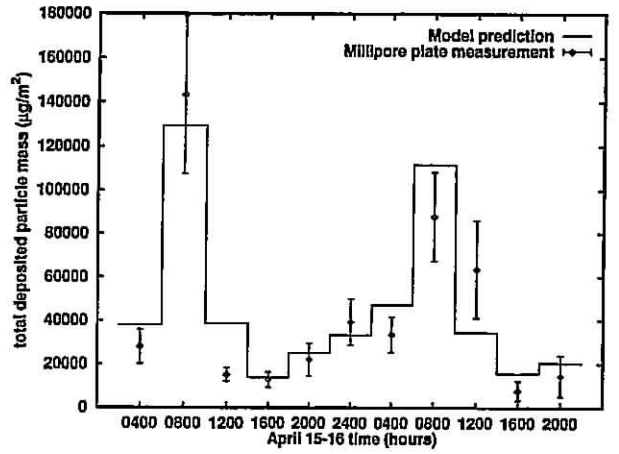

FIGURE 7. Model predictions versus measured values of the total particle mass flux per nominal 4-h sampling period deposited onto horizontal surfaces inside cave 9 over the period of April 15–16, 1991. Error bounds on the measured values equal 1 SD.

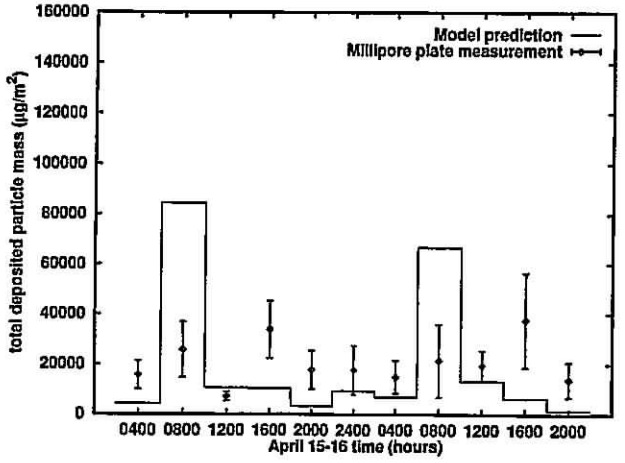

FIGURE 8. Model predictions versus measured values of the total particle mass flux per nominal 4-h sampling period deposited onto horizontal surfaces inside cave 6 over the period of April 15–16, 1991. Error bounds on the measured values equal 1 SD.

sources and the rapid removal of very large particles by sedimentation, often vary considerably over short distances. The entrances to cave 6 are located about 43 m away from the outdoor samplers, while the outdoor samplers are only 2 m away from the entrance to cave 9. Airborne particle concentration and deposition fluxes inside cave 6 also are more difficult to measure accurately because the lower concentrations and fluxes in cave 6 as compared to cave 9 yield smaller particle counts. In spite of this, the model predictions for coarse particles in cave 6 are within 2 standard errors of the measured value of the indoor aerosol size distribution and deposition flux data in most cases. Comparison of model predictions for airborne fine particle mass concentration obtained by integrating the predicted size distribution of Figure 6a below 2.1 μm diameter versus that measured by filtration yields good agreement (129 μg m^{-3} predicted vs 116 μg m^{-3} measured averaged over the 2-day experiment).

The time series of deposition flux predictions to horizontal surfaces inside caves 9 and 6 are shown in Figures 7 and 8, respectively. The deposition flux predictions inside cave 9 are in excellent agreement with measured values at most times. The deposition fluxes inside cave 6, both measured and predicted, differ considerably from those inside cave 9, because the early morning peak in the

TABLE 5

Deposition Fluxes to Surfaces inside Caves 6 and 9 at Buddhist Cave Temples at Yungang, April 15–16, 1991[a]

method	horizontal surfaces[b] ($\mu g\ m^{-2}\ s^{-1}$)	vertical surfaces ($\mu g\ m^{-2}\ s^{-1}$)	ceiling ($\mu g\ m^{-2}\ s^{-1}$)
	Cave 9		
measured	2.9		
modeled	3.0	7.12×10^{-4}	3.93×10^{-4}
	Cave 6		
measured	1.4		
modeled	1.4	5.41×10^{-5}	1.73×10^{-5}

[a] Note that the measured deposition fluxes over other time periods are higher. For the 21-day period April 12–May 1, 1991, the deposition fluxes averaged 13.40 and 4.54 $\mu g\ m^{-2}\ s^{-1}$ to horizontal surfaces in caves 9 and 6, respectively. Over the 1-yr period 1991–1992, the deposition fluxes to horizontal surfaces within cave 6 averaged 5.23 $\mu g\ m^{-2}\ s^{-1}$ (4). [b] Upward-facing horizontal surfaces.

deposition fluxes at cave 9 is suppressed both by the longer retention times for air exchange in cave 6 (about four times longer than in cave 9) and by the way that the wooden temple structure doors are operated at cave 6 (the outdoor particle inputs to the models for both caves are represented as being identical). Particle fluxes inside cave 6 are generally lower than at cave 9 at most times. The predicted particle fluxes in Figure 8 fall within 2 standard errors of the individual measurements at most times, yet there is evidence for some bias in the model or in the measurements, with model predictions falling below nominally measured values in 8 out of 11 sampling periods.

Model predictions of the integrated mass flux of particles to horizontal surfaces, to vertical surfaces, and to the ceiling of caves 6 and 9 are given in Table 5. Results are stated as a deposition flux converted to a 24-h average for the conditions that occurred on April 15–16, 1991. The horizontal fluxes can be compared to the measured values averaged over a 24-h day. The model predictions and measured values are in good agreement. It should be noted here that deposition fluxes over longer periods of time would have been larger. Measurements made over a 1-yr period in 1991–1992 show a deposition flux to horizontal surfaces for the year of 5.23 $\mu g\ m^{-2}\ s^{-1}$ in cave 6, which is a factor of 4 higher than observed during April 15–16, 1991 (4). Differences between the 2-day period examined in detail here versus the longer term annual flux are undoubtedly due to day-to-day fluctuations in outdoor particle concentrations and changes in the outdoor temperatures that drive air exchange through the caves. The model works well enough that it would probably track these changes well over long periods of time if the outdoor pollutant data and temperature data needed to exercise the model for long periods of time were acquired. While the model is fairly sophisticated, the model inputs needed are surprisingly few.

Predicted deposition fluxes to vertical surfaces and to the cave ceiling also are given in Table 5. Fluxes to these surfaces are orders of magnitude smaller than to horizontal surfaces. This is because deposition to horizontal surfaces is dominated by gravitational sedimentation of coarse dust particles while deposition to vertical surfaces and to the ceiling is dominated by convective diffusion and thermophoresis. Deposition velocities due to gravitational settling are much higher than those due to convective diffusion and thermophoresis under the conditions at Yungang.

TABLE 6

Predicted Time (yr) for 100% Coverage To Occur[a]

surface orientation	cave 6	cave 9
upward-facing horizontal	0.5	0.3
vertical	270	18
ceiling	830	26

[a] Values shown are based on outdoor particle concentrations and air exchange rates calculated using data for the April 15–16, 1991, period. Particle fluxes over an annual averaging period inside cave 6 are a factor of 4 higher than during the April 15–16 period of simulation, indicating that over long periods of time, the time for complete coverage to occur is probably one-fourth as long as shown here (4).

Furthermore, coarse particle mass concentrations greatly exceed fine particle concentrations at Yungang (5), again favoring higher deposition fluxes due to gravitational sedimentation as compared to convective deposition processes.

The size distribution of the deposited particles predicted by the model has been used to compute the time required to completely cover initially clean surfaces of various orientations with their first full monolayer of particles if particle deposition rates were to continue for long periods of time at the rates observed for April 15–16, 1991. For the purposes of constructing this index, a full monolayer coverage by deposited particles is reached at the point where particles having a cumulative projected cross-sectional area of 1 cm^2 have deposited onto 1 cm^2 of cave surface. Results are shown in Table 6. Cave 9, which lacks a wooden shelter in front of the cave at present, is directly exposed to the outdoor atmosphere. Under April 15–16, 1991, conditions horizontal surfaces inside cave 9 would become completely covered by a monolayer of dust in only 0.3 yr, while vertical surfaces and the decorated ceiling would require 18 and 26 yr, respectively, to reach the same degree of coverage. Cave 6, which is sheltered by the wooden temple front structure and which has lower air velocities along its walls and smaller wall-air temperature differences than in cave 9, would require longer to reach the first full monolayer coverage by particles, as shown in Table 6. The particle size distributions of the fluxes to the walls, floor, and ceiling differ from each other, and for that reason surface coverage rates given in Table 6 relative to mass deposition rates given in Table 5 differ between surfaces. Recognizing that the deposition rate to horizontal surfaces over an annual period is about four times higher than during the April 15–16 conditions studied here, the actual average elapsed time to reach a full monolayer coverage by deposited particles is probably about one-fourth as long as the values shown in Table 6.

The model for air circulation and particle deposition within the Buddhist cave Temples at Yungang is judged to render useful predictions of particle accumulation within the caves. The model can be used in the future to predict the relative effectiveness of particle filtration systems and/or altered ventilation rates on the particle deposition problem at the Yungang Grottoes.

Acknowledgments

This work was supported by a research agreement from the Getty Conservation Institute (GCI). The cooperation and assistance of the staff of the Yungang Grottoes and the State Bureau of Cultural Relics is gratefully acknowledged, including Huang Kezhong, Zhu Changling, Sheng Weiwei, Li Xiu Qing, Li Hua Yuan, Xie Ting Fan, Yuan Jin Hu, Huang Ji Zhong, Zhi Xia Bing, and Bo Guo Liang of the Shanxi Institute of Geological Sciences and Zhong Ying Ying from Taiyuan University. Assistance critical to this work was provided by the GCI and their consultants, and we especially thank Neville Agnew, Po-Ming Lin, Shin Maekawa, and Roland Tseng for their help.

Literature Cited

(1) Knauer, E. R. *Expedition* **1983**, *Summer*, 27–47.
(2) Holloway, M. *Sci. Am.* **1995**, *272* (5), 98–101.
(3) Cox, L. B. *The Buddhist Cave-Temples of Yün-Kang & Lung-Men*; The Australian National University: Canberra, Australia, 1957.
(4) Christoforou, C. S.; Salmon, L. G.; Cass, G. R. *Atmos. Environ.* **1994**, *28*, 2081–2091.
(5) Salmon, L. G.; Christoforou, C. S.; Cass, G. R. *Environ. Sci. Technol.* **1994**, *28*, 805–811.
(6) Christoforou, C. S.; Salmon, L. G.; Cass, G. R. Air exchange within the Buddhist cave temples at Yungang, China. *Atmos. Environ.* **1996**, *30*, 3995–4006.
(7) Churchill, S. W.; Chu, H. H. S. *Int. J. Heat Mass Transfer* **1975**, *18*, 1323–1329.
(8) Incropera, F. P.; DeWitt, D. P. *Fundamentals of Heat and Mass Transfer*; Wiley: New York, 1985.
(9) Nazaroff, W. W.; Cass, G. R. *Environ. Sci. Technol.* **1989**, *23*, 157–166.
(10) Gelbard, F.; Seinfeld, J. H. *J. Colloid Interface Sci.* **1980**, *78*, 485–501.
(11) Corner, J.; Pendlebury, E. D. *Proc. Phys. Soc. (London)* **1951**, *B64*, 645–654.
(12) Nazaroff, W. W.; Cass, G. R. *J. Aerosol Sci.* **1987**, *18*, 445–455.
(13) Davies, C. N. *J. Aerosol Sci.* **1979**, *10*, 477–513.
(14) Nazaroff, W. W.; Cass, G. R. *Environ. Int.* **1989**, *15*, 567–584.
(15) Ligocki, M. P.; Liu, H. I. H.; Cass, G. R.; John, W. *Aerosol Sci. Technol.* **1990**, *13*, 85–101.
(16) Dietz, R. N.; Cote, E. A. *Environ. Int.* **1982**, *8*, 419–433.
(17) Lin, J. J.; Noll, K. E.; Holsen, T. M. *Aerosol Sci. Technol.* **1994**, *20*, 239–252.

Received for review November 21, 1995. Revised manuscript received July 11, 1996. Accepted July 22, 1996.[⊗]

ES950875R

[⊗] Abstract published in *Advance ACS Abstracts,* October 1, 1996.